

Spiral vortices in a two-dimensional ferromagnet

A. B. Borisov

Institute of Metal Physics, 620219, Ekaterinburg, Russia

I. G. Bostrem and A. S. Ovchinnikov

Department of Physics, Ural State University, 620083, Ekaterinburg, Russia

(Received 28 March 2005; revised manuscript received 26 August 2005; published 24 October 2005)

We present a study of a class of exact solutions having a form of spiral vortices for an isotropic two-dimensional Heisenberg ferromagnet using a continuum theory and direct numerical simulations of the spin system on a square lattice. We find their features issued from the conservation laws and describe their interaction. Reasons behind the formation of the proper spin configurations on a square lattice are investigated.

DOI: [10.1103/PhysRevB.72.134423](https://doi.org/10.1103/PhysRevB.72.134423)

PACS number(s): 05.45.Yv, 67.57.Fg

I. INTRODUCTION

In the last two decades solitons, vortices, and other nonlinear excitations in low-dimensional magnets have attracted much interest. These excitations play an essential role in two-dimensional (2D) magnetism and contribute to breaking of the long-range order in 2D magnets. Magnetic vortices are important for the dynamical and thermodynamical properties of magnets, for a review see Refs. 1–3. Predictions of the Belavin-Polyakov theory⁴ for localized structures with a finite energy (instantons) observed much later experimentally⁵ gave rise to intensive investigations of solitons in 2D magnets.^{6–9}

Some years ago magnetic vortices have been directly observed in permalloy^{10–14} and Co magnetic nanodots.^{15–17} High-frequency dynamical properties of the vortex state magnetic dots have been probed by Brillouin light scattering of spin waves¹⁸ and x-ray imaging technique.¹⁹ In recent experiments the spin-wave modes excited by magnetic field pulses of small lithographically define disks with a spin vortex configuration are imaged using time-resolved magneto-optic Kerr microscopy²⁰ and phase sensitive Fourier transformation technique.²¹ Both axially symmetric dynamical modes showing concentric nodes and symmetry breaking azimuthal eigenmodes having azimuthal nodes have been observed. An analysis of the time and frequency dependencies²² of the modes demonstrates that for moderate field pulses and large magnetic elements (several tens of microns) the excitation spectrum is dominated by magnetostatic modes. However, as noted by the authors of Ref. 23, when the size of the elements is reduced or higher modes are excited, the exchange interactions can, in general, no longer be ignored and the dynamic response gradually changes from a purely magnetostatic to an exchange-dominated one. One of the aims of the paper is to show an existence of nonlinear modes both with circular and azimuthal nodes in a 2D isotropic ferromagnet obtained with an account only exchange interaction. These modes can be observed as spiral-like vortex configurations. In addition to a detailed study of the spiral solutions within both *XY* and Heisenberg models is of interest for the possible applications in the physics of liquid crystals, quantum Hall effect and in the study of biological systems featuring self-organized spiral structures.^{24,25}

In this paper, we present a study of the spiral vortices in the isotropic 2D ferromagnet using a continuum theory and direct numerical simulations of the spin system on a lattice. Our principal concern is to understand in detail the structure of the spiral patterns and to find out the reasons for their appearance. Real compounds are not ideal systems and lattice defects such as impurities, local fields, and anisotropy are present in any material sample. The effect of nonmagnetic impurities (vacancies) on vortex and vortex-antivortex structures has recently been studied for 2D magnetic models with *XY* symmetry.^{26–28} These investigations show that an ideal vortex or their pair formations are deformed if the vortex centers are near the vacancy. In the continuum limit an account of the impurities results in logarithmic singularities in the spin field. On the other hand, in the quantum field studies of 2D $O(N)$ models enjoying a continuous symmetry these classical configurations with the logarithmic singularities are known as “superinstantons.”²⁹ To produce these configurations “superinstanton” boundary conditions (SIBCs) were introduced. These consist of Dirichlet conditions of the boundary of the system, and the additional freezing of one spin in the center of the sample. It was argued that unlike to standard free, periodic, and Dirichlet boundary conditions SIBC do not possess a well defined perturbation expansion,^{30,31} which means that by fixing the spin in the center one can change the ground state of the system.

The paper is organized as follows. In Sec. II the continuum approximation based upon equations of nonlinear spin dynamics is presented. We briefly review the existing literature and show that the continuum isotropic Heisenberg model yields two types of static solutions. A class of exact solutions of the model, that are local minima of the classical energy, is obtained using a special linearization procedure. We find a harmonic function of initial dynamical variables obeying the linear Laplace equation. Then, an inverse transformation gives solutions of the initial nonlinear model as functions of the harmonic solutions of the Laplace equation. As a result, exact solutions for the 2D isotropic ferromagnet are generated where spiral vortices are of special interest. They are likely to be relevant for nonperfect systems with defects. Thus, it has been recently shown that vortices are attracted by a nonmagnetic impurity.³²

In Sec. III we consider numerical simulations of spin configurations predicted by the continuum theory. First we investigate spin textures for the planar xy model with the imposed SIBCs. We show that in the sector with topological charge $q=0$ the ground state is a logarithmic source of the strength α . We find how the strength depends on a turn of the fixed spin in regard to spins at the system edges and check the continuum theory prediction for the energy. We consider the simplest formation of such kind of logarithmic sources, a pair including two sources of opposite strengths α and $-\alpha$. Then we investigate the case when the structure takes an out-of-plane form. A numerical simulation gives the structures which are close to the nodal solutions of Heisenberg model. In the topological sectors $q \neq 0$ the ground state is either a planar logarithmic spiral (xy model) or a space spiral vortex with an out-of-plane form (Heisenberg model). We show that these spin configurations minimizing an energy with imposed SIBCs reproduce features predicted by the continuum theory well.

II. ANALYTICAL RESULTS

The model to be investigated is the isotropic spin- S Heisenberg ferromagnet defined by the Hamiltonian

$$H = - \sum_{p,n} J_{pn} \vec{S}_p \vec{S}_n, \quad (1)$$

where \vec{S}_p represents the spin operator at the site p of a 2D square lattice with the nearest-neighbor distance \vec{a} , and $J_{pn} = J \delta_{n,p+\vec{a}}$ ($J > 0$) are the nearest-neighbor exchange couplings. The nonlinear differential equations describing the dynamics of the model can be obtained by taking diagonal matrix elements of the equation of motion for the raising operator $S_p^+ = S_p^x + iS_p^y$

$$-i\hbar \frac{dS_p^+}{dt} = [H, S_p^+] \quad (2)$$

of the p th spin in spin-coherent representation $|\Omega\rangle = \prod_p |\theta_p, \phi_p\rangle$, where $0 \leq \theta_p \leq \pi$ and $0 \leq \phi_p < 2\pi$ parametrize the spin states on the unit sphere.³³ For the bilinear Hamiltonian this results in the system for the classical variables $\{\theta_p, \phi_p\}$ parametrizing the \vec{S}_p spin

$$\begin{aligned} \sin \theta_p \frac{\partial \phi_p}{\partial t} = & - \frac{S}{\hbar} \sum_n J_{np} \sin \theta_n \cos \theta_p \cos(\phi_p - \phi_n) \\ & + \sin \theta_p \frac{S}{\hbar} \sum_n J_{np} \cos \theta_n, \end{aligned} \quad (3)$$

$$\frac{\partial \theta_p}{\partial t} = \frac{S}{\hbar} \sum_n J_{np} \sin \theta_n \sin(\phi_n - \phi_p). \quad (4)$$

From hereon, n runs over the nearest neighbors. In the continuum limit we introduce the fields $\theta(x,y), \phi(x,y)$, which are defined in the (x,y) plane. The equation of motion for static solutions $\partial \theta_p / \partial t = \partial \phi_p / \partial t = 0$ can be obtained by applying the continuum approximation to the equation of spin motion on the discrete lattice. This yields

$$\Delta \theta = \sin \theta \cos \theta (\vec{\nabla} \phi)^2,$$

$$\vec{\nabla} (\sin^2 \theta \vec{\nabla} \phi) = 0. \quad (5)$$

A remarkable property of these equations is a conformal invariance that allows us to subdivide their static solutions into two groups. For the first group of solutions the expression

$$\frac{\partial \theta}{\partial x} \frac{\partial \phi}{\partial y} - \frac{\partial \theta}{\partial y} \frac{\partial \phi}{\partial x} \quad (6)$$

does not equal zero. Then we can obtain solutions from already known ones via conformal transformations. Indeed, $\theta_1(x,y), \phi_1(x,y)$ are some particular solutions of Eqs. (5). We may see by direct calculations that the fields $\theta_1[u_1(x,y), u_2(x,y)], \phi_1[u_1(x,y), u_2(x,y)]$ are also the solutions of the same system provided the $u_1 + iu_2$ is an arbitrary analytic function F of the argument $x+iy$

$$u_1 + iu_2 = F(x + iy). \quad (7)$$

Up to now, all known solutions belong to the first group. For this case $\phi(x,y)$ may be written in the simple form

$$\phi(x,y) = u_2(x,y), \quad (8)$$

and the another function θ depends only on the $u_1(x,y)$, i.e., $\theta_1[u_1(x,y), u_2(x,y)] = \theta_1(u_1)$, and obeys the simple equation of pendulum motion

$$\theta_{u_1, u_1}(u_1) = \frac{1}{2} \sin[2\theta(u_1)]. \quad (9)$$

The cases of the infinite and finite pendulum motions correspond to the following solutions:

$$\cos \theta(x,y) = \text{sn} \left[\frac{u_1(x,y)}{k}, k \right] \quad (0 < k < 1), \quad (10)$$

$$\cos \theta(x,y) = k \text{sn}[u_1(x,y), k] \quad (0 < k < 1), \quad (11)$$

where the Jacobi elliptic function of modulus k is used. Equations (8), (10), and (11) describe a set of quiescent topological defects centered at positions $z_i = x_i + iy_i$ (see Ref. 34) with

$$\begin{aligned} u_1(x,y) + iu_2(x,y) = & \sum_{i=1}^n \left(\frac{2ikK}{\pi} N_i + Q_i \right) \ln(x + iy - z_i) \\ & (N_i, Q_i \in \mathbb{Z}). \end{aligned} \quad (12)$$

Here, $K = K(k)$ is the complete elliptic integral of the first kind, and c_i are fixed complex parameters.

For $n=1$, $N_1=0$, and $k=1$ the solution of Eqs. (8) and (10)–(12)

$$\cos \theta(x,y) = \tanh u_1(x,y), \quad u_1 = Q \ln \sqrt{x^2 + y^2},$$

$$u_2 = Q \arctan \left(\frac{y}{x} \right)$$

coincides with the Belavin-Polyakov vortex (“baby” soliton)⁴ with the topological charge Q .

For $n=1$, $N_1 \neq 0$, $k \neq 1$ the solution of Eqs. (10) and (12) represents a N_1 -armed logarithmic spiral consisting of $2N_1$ spiral regions separated by the same number of logarithmic spiral walls.³⁴ The field $\varphi(x, y)$ (8) and (12) determined by the topological charge Q_1 does not alter along the logarithmic spiral curves in the (x, y) plane. Note that the spiral vortices in the ferromagnet, involving both θ and φ variables, have the different mathematical structure in comparison with the optical spiral vortices and the spiral vortex solution of the complex Landau-Lifshitz model³⁵ where only a φ angle is used to build proper configurations.

We are more interested in the second group of solutions when the expression (6) equals zero. In this case the angle $\varphi(x, y)$ is an arbitrary function of $\theta(x, y)$. Then we use the ansatz $\vec{\nabla}\varphi=f(\theta)\vec{\nabla}\theta$ to find solutions of this class with $\vec{\nabla}\varphi\parallel\vec{\nabla}\theta$. After eliminating the $\vec{\nabla}\varphi$ from [Eq. (5)], the equation for θ being

$$\sin\theta\frac{df}{d\theta}+2f\cos\theta+f^3\sin^2\theta\cos\theta=0. \quad (13)$$

This is Bernoulli equation in the variable $f(\theta)$, the general solutions are therefore given by

$$f(\theta)=\frac{1}{\sqrt{c^2\sin^4\theta-\sin^2\theta}}, \quad (14)$$

where $c^2>1$ is an arbitrary parameter. Inserting the ratio $\vec{\nabla}\varphi=f(\theta)\vec{\nabla}\theta$ and Eq. (14) into Eq. (5) we find the fields $\theta(\vec{r})$, $\varphi(\vec{r})$ as

$$\cos\theta=\frac{\sqrt{c^2-1}}{c}\cos a, \quad (15)$$

$$\varphi=\arctan(c\tan a)+\varphi_0,$$

where the field $a(x, y)$ is satisfied the Laplace equation

$$\Delta a=0. \quad (16)$$

We will only consider special case of solution for $a(x, y)$

$$a=\sum_{i=1}^n\alpha_i\ln\left(\frac{\sqrt{(x-x_{0i})^2+(y-y_{0i})^2}}{R_i}\right)+\sum_{i=1}^nq_i\arctan\left(\frac{y-\tilde{y}_{0i}}{x-\tilde{x}_{0i}}\right), \quad q_i\in\mathbb{Z}, \quad (17)$$

with the parameters α_i, q_i, R_i, c . In the above expression (x_{0i}, y_{0i}) and $(\tilde{x}_{0i}, \tilde{y}_{0i})$ are positions of sources and vortices, respectively, φ_0 is an initial value of azimuthal angle φ . We call the parameter α a strength of source that is identical to the term used in the hydrodynamic theory. From Eq. (15) we see that the parameter c governs out-of-plane spin components. In the soliton (15) the spins are confined to the vicinity of the xy plane with $\pi/2-\theta_{\max}\leq\theta<\pi/2+\theta_{\max}$ unlike the solutions of Eqs. (8), (10), and (12). The maximal value θ_{\max} is given by $\theta_{\max}=\arcsin\sqrt{c^2-1}/c$ for $n=1$. Equations (15) and (17) include well-known solutions considered earlier by some authors. Below, we list these cases.

(1) $n=1, c=1$ (pure in-plane solutions). Using Eq. (15) we find immediately that $\theta=\pi/2$ and $\varphi=q\phi+\alpha\ln(r/R)$ written in the polar coordinates r, ϕ . For $\alpha=0$ we restore Kosterlitz-Thouless (KT) vortices, and for $q=0$ we have ‘‘sources,’’ the equation for φ being $\varphi=\alpha\ln(r/R)$.^{29,36}

(2) $n=1, \alpha\neq 0, q=0$ (solutions with out-of-plane spin components). Equation (15) can be written as

$$\cos\theta=\frac{\sqrt{c^2-1}}{c}\cos\left(\alpha\ln\frac{r}{R}\right),$$

$$\varphi=\arctan\left[c\tan\left(\alpha\ln\frac{r}{R}\right)\right]+\varphi_0. \quad (18)$$

This agrees with the result obtained in Ref. 37 (‘‘nodal’’ solutions).

A new class of exact solutions

$$\cos\theta=\frac{\sqrt{c^2-1}}{c}\cos\left(\alpha\ln\frac{r}{R}+q\phi\right),$$

$$\varphi=\arctan\left[c\tan\left(\alpha\ln\frac{r}{R}+q\phi\right)\right]+\varphi_0 \quad (19)$$

are the two-dimensional spirals.³⁸ Figure 1 presents them for different parameters α and q . The former value assigns a spiral twist and the latter defines a number of spiral arms. For $\alpha=0$ we obtain a vortex with a nonzero out-of plane component

$$\cos\theta=\frac{\sqrt{c^2-1}}{c}\cos(q\phi),$$

$$\varphi=\arctan[c\tan(q\phi)]+\varphi_0. \quad (20)$$

Unlike the Skyrmion the soliton has a zero topological charge $\pi_2(S_2)=0$. Since θ does not depend on the radial coordinate r , the solution has no axial symmetry.

There are several conserved quantities that are important in what follows: the total energy E , the linear momentum \vec{P} , the angular momentum L_z , and the total number of spin reversals N (see, e.g., Ref. 39).

The energy of the soliton given by Eq. (15) can be evaluated in continuum approximation resulting in a more compact form

$$E=\frac{1}{2}JS^2\int d\vec{r}(\vec{\nabla}a)^2. \quad (21)$$

Using Eq. (17) for the function a we obtain

$$E=\pi JS^2\left\{\sum_i(\alpha_i^2+q_i^2)\ln\frac{L}{r_0}+\sum_{ij}(\alpha_i\alpha_j+q_iq_j)\ln\frac{L}{d_{ij}}\right\}, \quad (22)$$

$d_{ij}=\sqrt{(x_{0i}-x_{0j})^2+(y_{0i}-y_{0j})^2}$ is a distance between i th and j th vortices, L is a size of the system, and r_0 is a cutoff radius where the continuum approximation breaks down. After the formal substitution $q_iq_j\rightarrow\alpha_i\alpha_j+q_iq_j$ in Eq. (22) we recognize the energy of interacting in-plane vortices. We note the

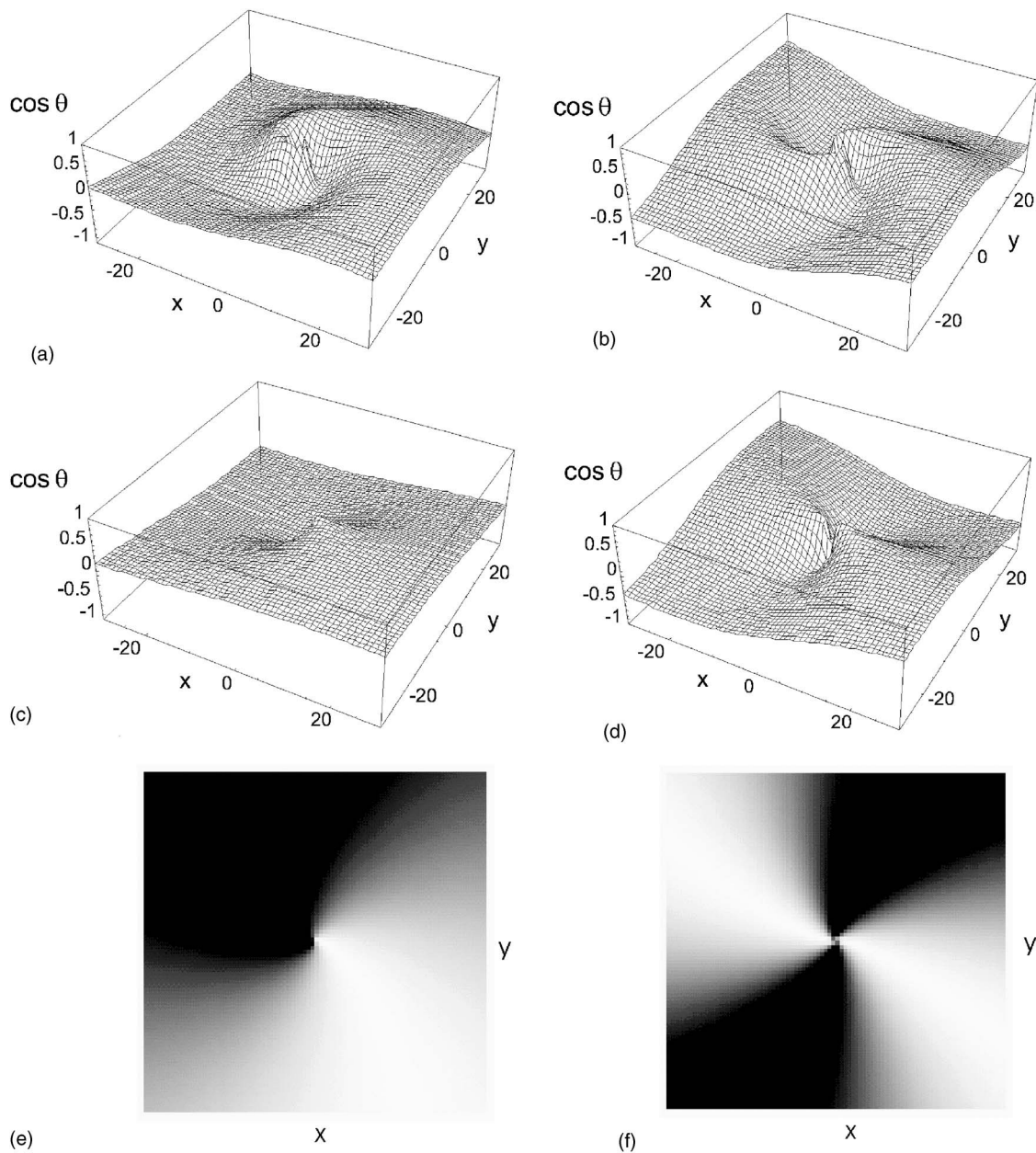


FIG. 1. Spiral vortices with $\alpha=2.0$ [$q=1$ (a), $q=2$ (b)] and with $\alpha=0.3$ [$q=1$ (c), $q=2$ (d)]. Density images of the amplitude and the phase of the magnetization are given for the last set. The map (e) has one node curve dividing the bright-dark regions of equal amplitude but opposite phase. The map (f) consists of four regions, oscillating in pairs in phase. Note a similarity of topological small- α spiral vortices with dynamical magnetostatic nonaxially symmetric modes (see Fig. 1 in Ref. 23) and Figs. 3 and 4 in Ref. 21.

absence of terms $\alpha_i q_j$. One can see that vortices and sources do not interact with each other. The parameters R_i and c do not enter into the expression at all.

Two spiral vortices of opposite values (α, q) and $(-\alpha, -q)$ with a pair separation d has the finite energy

$$E = 2\pi JS^2(\alpha^2 + q^2)\ln\left(\frac{d}{r_0}\right)$$

meaning that these vortices may be bound in pairs.

Next we derive another conserved quantities related with the spiral vortex. The density of momentum is determined by the formula

$$\vec{P} = \frac{\hbar S}{c + \sqrt{c^2 - 1} \cos a} \vec{\nabla} a$$

consisting of the radial

$$P_r = \frac{\hbar S}{c + \sqrt{c^2 - 1} \cos a} \frac{\alpha}{r} \tag{23}$$

and the azimuthal

$$P_\phi = \frac{\hbar S}{c + \sqrt{c^2 - 1} \cos a r} \frac{q}{r} \quad (24)$$

parts. The P_r and P_ϕ components are defined by the twist parameter α and the vorticity q , respectively. Substituting Eqs. (23) and (24) in the relations

$$\begin{aligned} \int_0^{2\pi} P_r R_0 d\phi &= \alpha \hbar S \int_0^{2\pi} d\phi \frac{1}{c + \sqrt{c^2 - 1} \cos\left(q\phi + \alpha \ln \frac{r}{R}\right)} \\ &= 2\pi \alpha \hbar S \end{aligned}$$

and

$$\begin{aligned} \int_0^{2\pi} P_\phi R_0 d\phi &= q \hbar S \int_0^{2\pi} d\phi \frac{1}{c + \sqrt{c^2 - 1} \cos\left(q\phi + \alpha \ln \frac{r}{R}\right)} \\ &= 2\pi q \hbar S \end{aligned}$$

we clarify the physical meaning of the quantities α and q . The first constraint is related with a flow of the momentum through the circle of the radius R_0 surrounding the vortex core and the last one determines a quantized circulation along the circle.

The total orbital angular momentum L_z along the rotation axis through the area πL^2 here reads as

$$\begin{aligned} L_z &= S \hbar q \int_0^L r dr \int_0^{2\pi} d\phi \frac{1}{c + \sqrt{c^2 - 1} \cos\left(q\phi + \alpha \ln \frac{r}{R}\right)} \\ &= S \hbar q \pi L^2, \end{aligned}$$

where the density of the angular momentum is defined as

$$\frac{S \hbar q}{c + \sqrt{c^2 - 1} \cos\left(q\phi + \alpha \ln \frac{r}{R}\right)}.$$

The total linear momentum amounts here to $\int \vec{P} d^2 r = 0$.

The conservation of total number of spin reversals (magnon density)

$$N = S \left[1 - \frac{\sqrt{c^2 - 1}}{c} \cos\left(\alpha \ln \frac{r}{R} + q\phi\right) \right] \quad (25)$$

involves the magnon density current

$$\vec{j} = \frac{JS^2}{\hbar c} \left(\frac{q}{r} \vec{e}_\phi + \frac{\alpha}{r} \vec{e}_r \right). \quad (26)$$

From Eqs. (23) and (26), it follows that the presence of additional terms with a nonzero strength of source α produces radial components in the densities of the momentum \vec{P} and the magnon current \vec{j} .

To complete our analytical study we discuss stability of the spiral vortices. Given the energy (21) we would like to consider the effect of perturbation $\delta\psi$, that belongs to the same class as the $a(x, y)$ does, on the soliton structure [Eq. (15)]. This yields

$$\begin{aligned} E[a + \delta\psi] &= \frac{1}{2} JS^2 \int d\vec{r} (\vec{\nabla} a + \vec{\nabla} \delta\psi)^2 = \frac{1}{2} JS^2 \int d\vec{r} [(\vec{\nabla} a)^2 \\ &+ 2(\vec{\nabla} a)(\vec{\nabla} \delta\psi) + (\vec{\nabla} \delta\psi)^2] = \frac{1}{2} JS^2 \int d\vec{r} [(\vec{\nabla} a)^2 \\ &+ (\vec{\nabla} \delta\psi)^2] > E[a], \end{aligned}$$

i.e., the system pays an energy cost and the soliton turns out to be stable against the small perturbations of the field $a(x, y)$.

Among the several questions that should be arisen in the above analysis, an origin of logarithmic sources and a range of possible values of α parameter are ones of the most important. Due to the intrinsic interest, an analysis of physical reasons behind the formation of spiral vortices is called for. In addition, the continuum theory cannot completely describe subtle differences occurring on the lattice at short length scales. Therefore we should concern how to organize a numerical process leading to spin configurations that may be compared with the spiral vortices. We are aware of the difference between these spin patterns and spiral vortices predicted by the continuum theory. In the first case we deal with a ground state of the system under certain constrains and in the other case with stationary nonlinear excitations. Our studies will involve lattice model on 2D square lattice. Ultimately, a lattice model is the original source of any continuum theoretical description. We will then compare the continuum theory predictions to results found in numerical calculations.

III. NUMERICAL SIMULATIONS

A. The model

To describe in full detail the method of numerical simulations we rewrite the system (3) and (4) in the form convenient for an iteration procedure. From Eq. (4) we get

$$\cos \varphi_p \left(\sum_n J_{np} \sin \theta_n \sin \varphi_n \right) = \sin \varphi_p \left(\sum_n J_{np} \sin \theta_n \cos \varphi_n \right)$$

that yields

$$\begin{aligned} \sin \varphi_p &= \pm \frac{\sum_n J_{np} \sin \theta_n \sin \varphi_n}{\sqrt{(\sum_n J_{np} \sin \theta_n \sin \varphi_n)^2 + (\sum_n J_{np} \sin \theta_n \cos \varphi_n)^2}}, \end{aligned} \quad (27)$$

cos φ_p

$$\begin{aligned} &= \pm \frac{\sum_n J_{np} \sin \theta_n \cos \varphi_n}{\sqrt{(\sum_n J_{np} \sin \theta_n \sin \varphi_n)^2 + (\sum_n J_{np} \sin \theta_n \cos \varphi_n)^2}} \end{aligned} \quad (28)$$

and the upper sign must be taken for a ferromagnet ($J_{np} > 0$). Similar equation for θ_p is obtained from Eq. (3) which can be written as

$$\sin \theta_p \left(\sum_n J_{np} \cos \theta_n \right) = \cos \theta_p \sum_n J_{np} \sin \theta_n (\cos \varphi_n \cos \varphi_p + \sin \varphi_n \sin \varphi_p). \quad (29)$$

Application of Eqs. (27) and (28) to this equation gives

$$\cos \theta_p = \sin \theta_p \frac{\sum_n J_{np} \cos \theta_n}{\sqrt{(\sum_n J_{np} \sin \theta_n \sin \varphi_n)^2 + (\sum_n J_{np} \sin \theta_n \cos \varphi_n)^2}} \quad (30)$$

that after some simplifications yields the expression used in a numerical algorithm

$$\cos \theta_p = \frac{\sum_n J_{np} \cos \theta_n}{\sqrt{(\sum_n J_{np} \cos \theta_n)^2 + (\sum_n J_{np} \sin \theta_n \sin \varphi_n)^2 + (\sum_n J_{np} \sin \theta_n \cos \varphi_n)^2}}. \quad (31)$$

Together with Eq. (30) it implies $\sin \theta_p > 0$.

In actual practice, the spin configuration was found by using the original lattice spin fields \vec{S}_n and iteratively reorienting each along the effective local field due to its neighbors. Scanning linearly through the lattice each site was updated in sequence, being reset along the net field due partly to some unchanged neighbors and some that have already been reoriented. This gives fast convergence than a synchronized global update. The iterations stop if the sum

$$\sigma = \sqrt{\sum_{i,j=0}^N (\sin \theta_{ij}^{(k)} - \sin \theta_{ij}^{(k-1)})^2 + \sum_{i,j=0}^N (\sin \varphi_{ij}^{(k)} - \sin \varphi_{ij}^{(k-1)})^2} \quad (32)$$

taken over a quarter of the lattice on the k th step is less than tolerance 10^{-6} – 10^{-10} . We employed the lattice coordinates in Eq. (32) for the notation of site indices.

The most difficult computational problem in carrying out this program is to find the initial configuration that relaxes to a target spin configuration. It is meaningful to impose appropriate boundary conditions too. Obviously this a rich problem with a wide choice of options.

One way is to take the configuration according to the continuum formula and assume that each spin has small amplitude dynamic deviations from the starting structure. Another approach has been used in a study of a single magnetic vacancy centered in vortex.²⁸ For numerical calculations a finite core circular system of radius R_c is taken. Lattice sites are set up surrounding the origin and only those within radius R_c are kept. A detailed discussion of starting configurations needed for a finding of proper lattice structure and boundary conditions adopted in calculations will be given in every case. We note here, they are essentially different for vortex, logarithmic, and spiral spin arrangements and their pairs.

Another important point of numerical simulations is a criteria of consistent between the relaxed spin configuration and an appropriate continuum solution. We suggest the following scheme for the comparing. (i) The continuum theory is not relevant to spins at sites close to the vortex core. Far from the core the relaxed spin angles must well be described by

the continuum formula. Thus, we have to control this coincidence with a prescribed precision in a region where the continuum description works. (ii) The number of independent parameters in a continuum solution must be the same as a number of corresponding degrees of freedom controlled in numerical simulations. (iii) A relaxed configuration should not lose the symmetry of continuum solution, i.e., it should have a similar dependence on the space coordinates (r, ϕ) . (iv) In addition, we confirm the finding of proper solution by analyzing the total energy of a relaxed configuration

$$E = \frac{S^2}{2} \sum_{n,p} J_{np} [\sin \theta_n \cos \theta_p \cos(\varphi_p - \varphi_n) + \cos \theta_p \cos \theta_n]$$

comparing it with a continuum theory prediction.

B. Logarithmic source

1. XY model

Our current aim is to perform simulations of a logarithmic source in the planar XY model. The static in-plane angles satisfy the discrete nonlinear equations

$$\sin \varphi_p = \frac{\sum_n J_{np} \sin \varphi_n}{\sqrt{(\sum_n J_{np} \sin \varphi_n)^2 + (\sum_n J_{np} \cos \varphi_n)^2}}, \quad (33)$$

$$\cos \varphi_p = \frac{\sum_n J_{np} \cos \varphi_n}{\sqrt{(\sum_n J_{np} \sin \varphi_n)^2 + (\sum_n J_{np} \cos \varphi_n)^2}} \quad (34)$$

drawn from Eqs. (27) and (28) after the substitution $\sin \theta_n = 1$.

A homogeneous arrangement $\varphi_p = \varphi = \text{const}$ is an obvious solution of these equations for any set of the exchange couplings J_{np} . An attempt to carry out numerical simulations using a magnetic vacancy with some zero nearest-neighbor exchange couplings, a magnetic impurity with another spin and/or different exchange leads to the uniform arrangement and does not permit to get a structure similar to a logarithmic solution

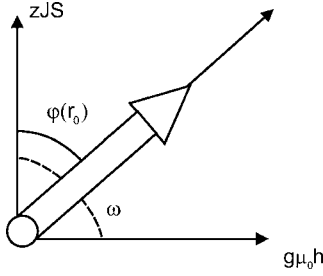


FIG. 2. Core spin (white arrow) points along an axis determined jointly by the exchange field zJS of the nearest neighbors and the local field h .

$$\varphi = \varphi_0 + \alpha \ln \frac{r}{R}. \quad (35)$$

A close examination of an in-plane arrangement given by the analytical model shows that there is some bending of spins in the center with reference to spin order in the vicinity of the system edges. This nonuniformity of spin distribution can gain insight into the numerical process driving the starting spin configuration to desired in-plane structure. A reason behind the formation of the nonuniformity may be either a local magnetic field or a local anisotropy. We fix our attention on the first case. Indeed, an inclusion into the Hamiltonian of the local field h , acting on a spin at position \vec{r}_0 , whose direction relative to fixed spins at boundary is determined by the angle ω (see Fig. 2)

$$H_z = -g\mu_0 h S \int d\vec{r} \delta(\vec{r} - \vec{r}_0) \cos[\omega - \varphi(\vec{r})] \quad (36)$$

leads to the continuum equation

$$\Delta \varphi(\vec{r}) = \frac{g\mu_0 h}{JS} \sin[\omega - \varphi(\vec{r})] \delta(\vec{r} - \vec{r}_0). \quad (37)$$

It then follows that

$$\varphi(\vec{r}) = \varphi_u(\vec{r}) + \frac{g\mu_0 h}{2\pi JS} \sin[\omega - \varphi(\vec{r}_0)] \ln |\vec{r} - \vec{r}_0|, \quad (38)$$

where φ_u is an arbitrary solution of the Laplace equation $\Delta \varphi_u = 0$ in two dimensions. A comparison of the result with Eq. (35) yields

$$\alpha = \frac{g\mu_0 h}{2\pi JS} \sin[\omega - \varphi(\vec{r}_0)]. \quad (39)$$

We can proceed and estimate the expression using consideration of the mean-field theory. Taking $\omega = \pi/2$ and suggesting that all the spins are aligned parallel to the one direction except the core spin, pointed fixedly along an axis determined both the exchange field zJS of the nearest neighbors and the local field h , we easily find

$$\sin[\omega - \varphi(\vec{r}_0)] = \frac{zJS}{\sqrt{(zJS)^2 + (g\mu_0 h)^2}}, \quad (40)$$

where z is the number of nearest neighbors. Therefore,

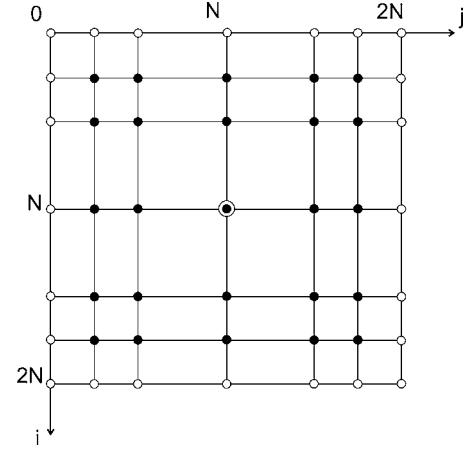


FIG. 3. Coordinates (i, j) for square lattice. The core spin is denoted by white-black circle. Solid circles indicate the inner sites involved into iteration procedure. Open circles are the boundary sites.

$$\alpha = \frac{z}{2\pi} \frac{g\mu_0 h}{\sqrt{(zJS)^2 + (g\mu_0 h)^2}}. \quad (41)$$

As we can see α ranges from 0 to $z/2\pi \approx 0.636$ when h increases from zero to infinity. Most importantly, the local magnetic field is the reason of an appearance of the logarithmic source in the system and there is the upper limit for α values.

To check the predictions with the numerical simulation data we consider a square lattice of size $(2N+1) \times (2N+1)$ shown in Fig. 3 and take $J_{np} = J$ for simplicity. We carry out the iteration process beginning from one of the corners of the lattice. Let the local magnetic field directed along the j axis act on a core spin which has the coordinates (N, N) [Fig. 4(a)]. This spin should be included into the numerical scheme [Eqs. (33) and (34)] with a little modification

$$\cos \varphi_{NN} = \frac{\sum_n \cos \varphi_n + g\mu h / (JS)}{\sqrt{(\sum_n \sin \varphi_n)^2 + [\sum_n \cos \varphi_n + g\mu h / (JS)]^2}}. \quad (42)$$

During the iterations a turn of the central spin $\varphi(\vec{r}_0)$ proportional to the applied field h is seen to develop in regard to uniform arrangement at the boundaries which hold fixed and are not updated during the iterations [Fig. 4(b)].

It is important to establish that our analytical model reproduces the results obtained by numerical simulations. On a lattice the in-plane angles φ_n deviate from the formula (35) and obtain modifications largest near the core spin. These angles satisfy a discrete Laplace equation

$$\sum_{\delta} \sin(\varphi_n - \varphi_{n+\delta}) = 0 \quad (43)$$

issued from Eq. (4).

Similar to the analytical prediction, we find that the radial dependence of the arrangement is mostly preserved, φ_n is determined only by an absolute distance r measured from the

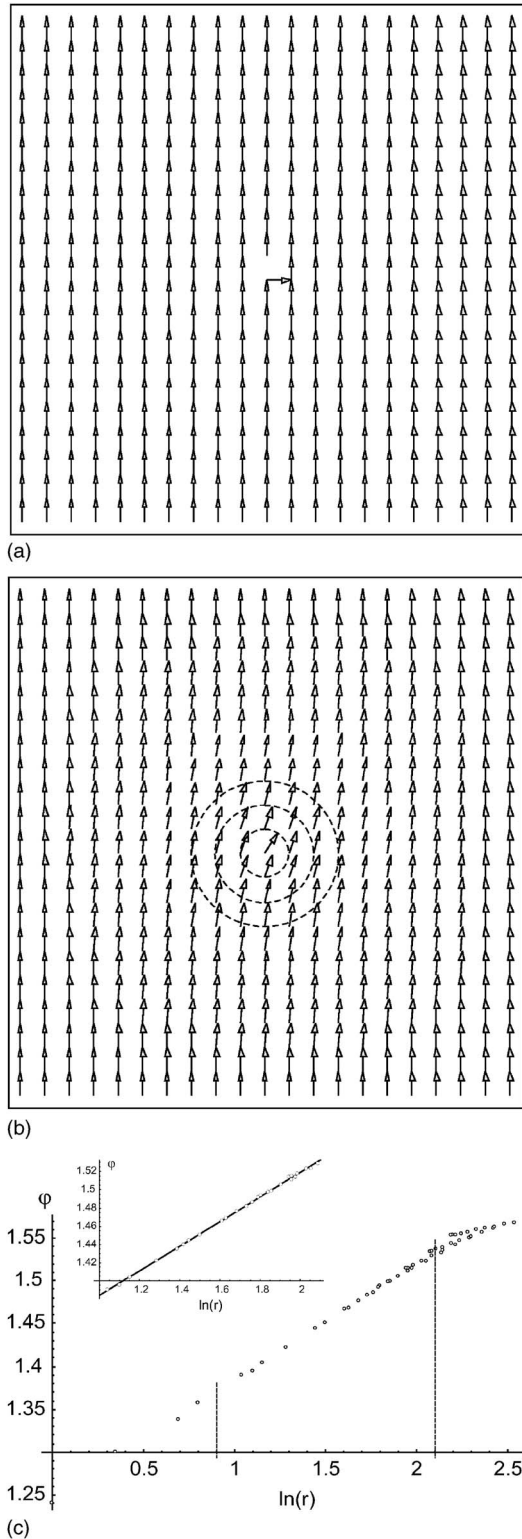


FIG. 4. Starting configuration used to get a logarithmic source (a) and equilibrium configuration obtained in the iteration procedure (b). Core spin is placed at position (10, 10). The final equilibrium state reached after 50 000 iterations with an accuracy 10^{-15} . A comparison between the numerical simulation (points) and the analytical model (lines). To exclude the lattice artifacts due to fixed boundary conditions we use the points with $1 \leq \ln r \leq 2$ for the fitting shown in the inset (c).

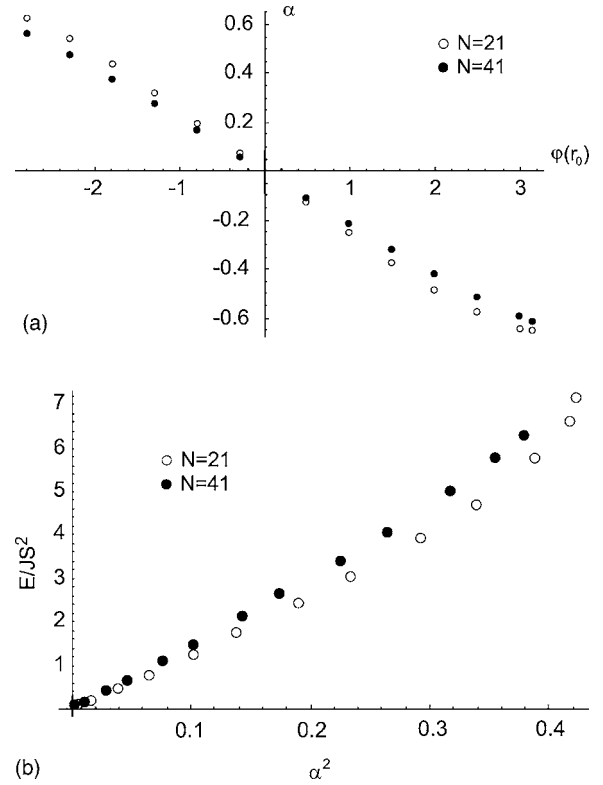


FIG. 5. The α value as a function of $\varphi(r_0)$ (a) and the energy E as a function of α^2 (b). Note that the maximal α values found for different lattice sizes, $\alpha_{\max}=0.650$ ($N=21$) and $\alpha_{\max}=0.615$ ($N=41$), are close to the estimation 0.636 of the mean-field theory.

core site (N, N) beginning with $r \sim 3$. Figure 4(c) compares the numerical calculations performed for different scan directions with the analytical values given by Eq. (35). The points in the inset are fitted by $\varphi = \pi/2 + 0.135 \ln(r/10.84)$. The mean-field approximation (41) would give $\alpha = 2/\sqrt{17}\pi \approx 0.154$, where the magnetic field is $g\mu h/(JS) = 1$. One sees that the agreement is very good.

It makes sense to explore on a lattice the dependence $\alpha[\varphi(\vec{r}_0)]$. Instead of inclusion of local in-plane magnetic field the following simple but effective scheme was applied to enforce a desired logarithmic source position. Again a square lattice is used with a fixed spin at its center. This core spin with a given $\varphi(\vec{r}_0)$ would be excluded from updating in the numerical routine. In order to find a range of values for the coefficient α we investigate systems of size 21×21 and 41×41 . Figure 5(a) summarizes the results found from the relaxed configurations φ_{ij} with different starting deviations $\varphi(\vec{r}_0)$ by showing α as a function of $\varphi(\vec{r}_0)$. One sees the dependence is almost linear. The numerical α values for $N = 21, 41$ are slightly different, i.e., α weakly depends on the lattice size. The results indicate that relevant α values are small, i.e., $|\alpha| < 1$. More significantly, the analytical model only contains two parameters α and R and a relaxed spin configuration, obtained numerically, can only depend upon two independent variables $\varphi(\vec{r}_0)$ and N .

We then used the numerical code to calculate the energy of the structure

$$\frac{E}{JS^2} = \frac{1}{2} \sum_{np} \cos(\varphi_n - \varphi_p) + \sum_n \cos(\varphi_n - \varphi_0) - E_0, \quad (44)$$

where the first sum runs over all inner sites and the sum in the second term goes over the boundary sites that belongs to the structure. The energy was calculated relative to the ground-state energy E_0 , an amount of JS^2 per exchange bond, for spins aligned with an uniform angle φ_0 within the xy plane. The energy found as a function of α^2 , taken from the fitting, is linear right up to a maximal value α_{\max} corresponding to $\varphi(\vec{r}_0) = \pi$ that well agrees with the continuum model [Fig. 5(b)].

2. Pair of logarithmic sources

It is interesting to confirm the results found above by analysis an assembly of such kind of logarithmic sources. According to the continuum model, the simplest formation is a configuration including two sources of strength α and $-\alpha$

$$\begin{aligned} \varphi &= \frac{\alpha}{2} \ln \frac{(x-x_1)^2 + (y-y_1)^2}{R_1^2} - \frac{\alpha}{2} \ln \frac{(x-x_2)^2 + (y-y_2)^2}{R_2^2} \\ &= \phi_0 + \frac{\alpha}{2} \ln \frac{(x-x_1)^2 + (y-y_1)^2}{(x-x_2)^2 + (y-y_2)^2}, \end{aligned} \quad (45)$$

where $\phi_0 = \alpha \ln(R_2/R_1)$. The energy of the pair

$$E = 2\pi\alpha^2 JS^2 \ln d \quad (46)$$

is finite and have no dependence on system size.

We use a square system of size $2N+1$ with two sources placed symmetrically near its center which has the coordinates (N, N) . We found in the numerical studies that only distance between the sources and their mutual orientation on a lattice affect the values of energy and α . We present here our results obtained from simulations when the sources are placed at positions $(N-d/2, N)$ and $(N+d/2, N)$, where d is a distance between them. Alternatively, if the sources were placed at different positions away from the system center a boundary energy that changes significantly with the pair positions would result. To avoid this complication, it is much simpler to fix the source positions at the system center.

We investigate how the strength of source α could depend on the pair distance d and on a difference between the core spin angles $\delta\varphi = \varphi(r_{20}) - \varphi(r_{10})$ and how the analytical predictions for the energy ($E \sim \alpha^2$, $E \sim \ln d$) are modified on a lattice. The calculation required a larger system than for the previous case in order to produce stable configuration in a finite scale. We checked the finite size effects by simulating 21×21 to 1001×1001 square lattices. In addition, in the calculations presented here we control a restoring of homogeneous arrangement at system edges. The analytical solution (45) involves two independent parameters, i.e., the strength α and the distance d . In numerical simulations a number of independent quantities involved in the calculation is the same. The first parameter is determined by the difference $\delta\varphi$ and the second one is given explicitly via the source positions.

It is of importance to determine an optimal size of the system to avoid impractically long simulations for large

TABLE I. Data of numerical simulations for pair of logarithmic sources.

Size	E/JS^2	α	φ_0
21×21	15.9945	0.203	1.562
51×51	15.9984	0.127	1.569
31×31	15.9973	0.160	1.567
101×101	15.9988	0.108	1.5703
201×201	15.9989	0.1005	1.5707
301×301	15.9989	0.1005	1.5707

enough lattice. In the Table I some of the data, answering the purpose, is collected. The binding energies, the strength of source α and a relaxed background arrangement φ_0 are summarized there. As a starting configuration we take two spins at the distance $d=4$ turned almost oppositely to another magnetic moments. We run then iteration procedure to obtain equilibrium configuration. Fitting to the known solution (45) allows the determination of the needful quantities. One see that the background arrangement φ_0 does not approach the exact value $\pi/2$ when decreasing the size of the lattice ($L \leq 101$). Size effects are noticed for the strength of source α which becomes greater for small lattices. Increasing the L from 201 to 301 does not have an effect on α no φ_0 . As a rule of thumb, we hold the finite-size effects are negligible when $L \geq 50d$.

To compare the analytical expression (45) with a target in-plane arrangement (Fig. 6) we choose a scan along a path in the $(0,1)$ direction of the lattice, beginning with the point of one of the source. Similar results could be obtained along other scan directions, but with a worse consistence with the analytical predictions, since the region, where the continuum model is expected to be valid, is not isotropic. A fit of data points according to Eqs. (45) and (46) provides estimates for the parameter α and the energy E .

The dependence α on $\delta\varphi$ was examined for several d values. We found that the observed dependence is distinguished for small ($d=2-4$) and large ($d \geq 6$) pair distances.

For sufficiently small distances ($d \leq 4$) the pair presents an unit formation and cannot be treated adequately by the continuum model. A typical result for the energy obtained for a square lattice of size $L=141$ is shown in Fig. 7. The parameter α found as a function of $\delta\varphi$ is shown in Fig. 7(a). One sees that the dependence exhibits a clear periodical behavior. Due to the fact, the dependence $E(\alpha^2)$ calculated with the same data and plotted in Fig. 7(b) turns out to be nonlinear and many valued.

By contrast, for the large distances ($d > 10$) the agreement between the analytical model and the numerical simulations ($L=701$) is good enough. In Fig. 8(a) we show α as a function of $\delta\varphi$. The dependence is almost linear and this behavior is similarly observed for one logarithmic source. The energy of the pair as a function of α^2 also supports the agreement, E is directly proportional to α^2 until $\delta\varphi \approx \pi$ [Fig. 8(b)].

3. Nodal solutions of the Heisenberg model

The patterns which we have so far studied have been confined in the xy plane. A particularly interesting and complex

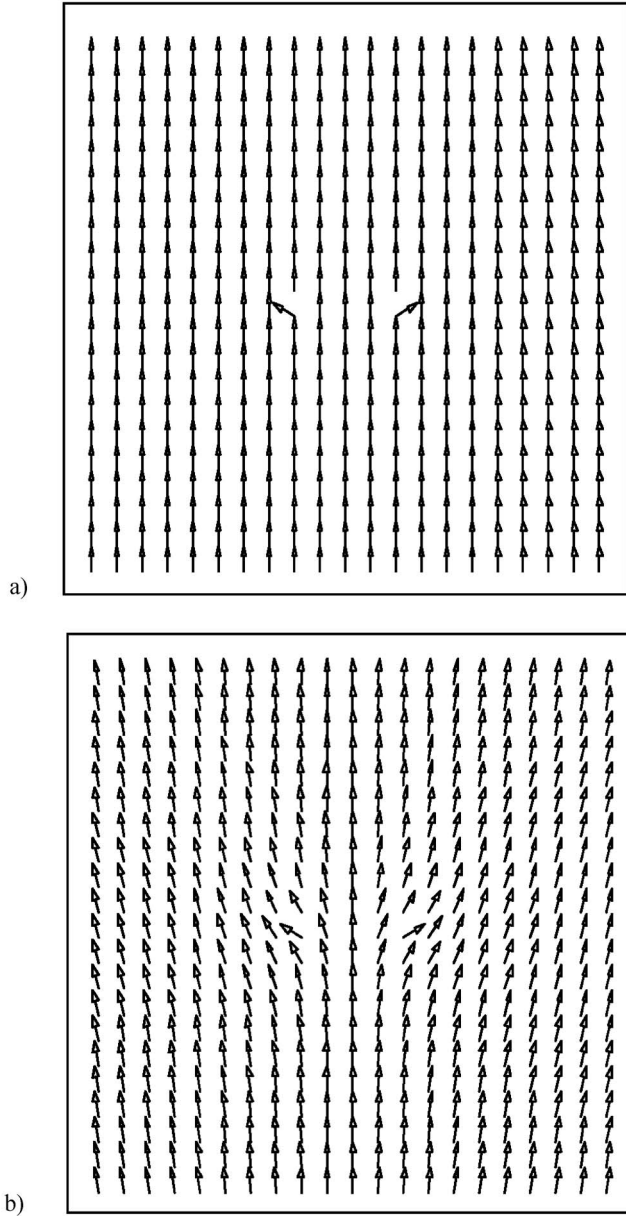


FIG. 6. Starting configuration used to get a pair of logarithmic sources (a) and relaxed configuration obtained in the iteration procedure with an accuracy $\sim 10^{-7}$ (b). In the starting configuration the in-plane angles of the selected sites are set equal to $\pi/2 + \delta\varphi/2$ and $\pi/2 - \delta\varphi/2$ and they are held fixed during the iteration scheme [Eqs. (33) and (34)]. The spins at the edges of the system have been included into the iteration procedure too and they have no constraint from outside, that is a free boundary condition holds. For all other spins, the in-plane angles are supposed to be $\pi/2$.

case is when the structure takes an out-of-plane form. Here we report numerical simulations of nodal states. The lattice is taken as in Fig. 3, however, in the initial configuration the pinned spin in the center has an out-of-plane component. The numerical procedure recurs those used for one logarithmic source and generates both a set $(\cos \varphi_{ij}, \sin \varphi_{ij})$ and $(\cos \theta_{ij}, \sin \theta_{ij})$. This allows us to extract from these simulations parameters involved in analytical expressions such as those derived in Sec. I.

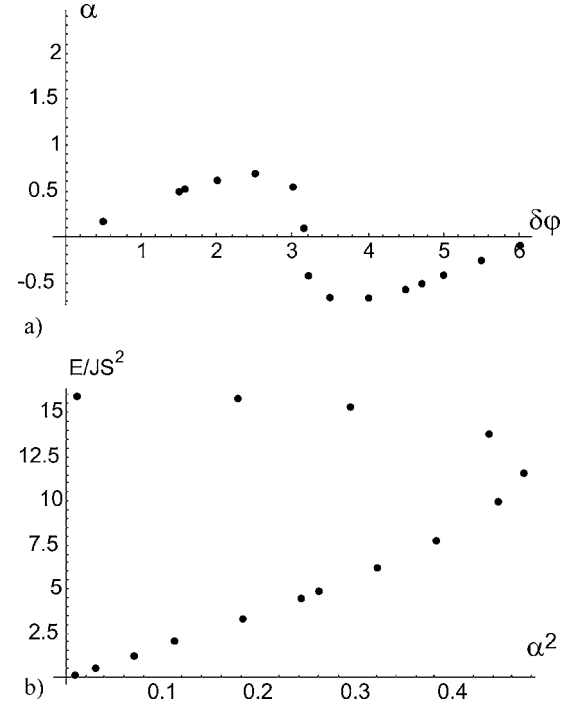


FIG. 7. Parameter α as a function of $\delta\varphi$ (a) and energy E as a function of α^2 (b) for a small-distance pair ($d=4$). The pair presents an unit formation and cannot be treated adequately by the continuum model.

Given a set of angles found numerically, we should summarize the data by fitting it to the model (18) that depends on the adjustable parameters φ_0 , c , α , and R , and the fit supplies the appropriate coefficients. To carry out the comparison we follow two steps. From Eqs. (18) we obtain

$$\sqrt{c^2 - 1} \cos \varphi_0 \cos \varphi_{ij} + \sqrt{c^2 - 1} \sin \varphi_0 \sin \varphi_{ij} = \tan \theta_{ij}. \quad (47)$$

Fitting Eq. (47) to the resulting spin structure by the least-square method, we obtain c and φ_0 . The rest parameters α and R are then adjusted to data for $\cos \theta$. We estimate

$$\varphi_{ij} = \tan^{-1} \left\{ c \tan \left(\alpha \ln \left[\frac{r_{ij}}{R} \right] \right) + \varphi_0 \right\}$$

with α , R , c , and φ_0 and compare φ_{ij} with numerical data points (Fig. 9). One sees that the agreement is rather good.

A set of numerical simulations was performed using different initial conditions for boundary $\vec{S}_b = (\sin \theta_b \cos \varphi_b, \sin \theta_b \sin \varphi_b, \cos \theta_b)$ spins and the central pinned spin $\vec{S}_c = (\sin \theta_c \cos \varphi_c, \sin \theta_c \sin \varphi_c, \cos \theta_c)$. We also used the expressions (18) as fitting formulas. These fits give us values for the strength α and the energy E listed in Table II. We found a significant signature: the α value is determined only by the angle $\Delta_{bc} = \cos^{-1}(\vec{S}_b \vec{S}_c)$ for any direction \vec{S}_c . To check this assertion we repeat calculations of Sec. III B 1 for the pure in-plane case with the starting deviations $\varphi(\vec{r}_0) = \Delta_{bc}$. A fit of data points according to Eqs. (35) and (44) gives the estimates for strength of source α and the

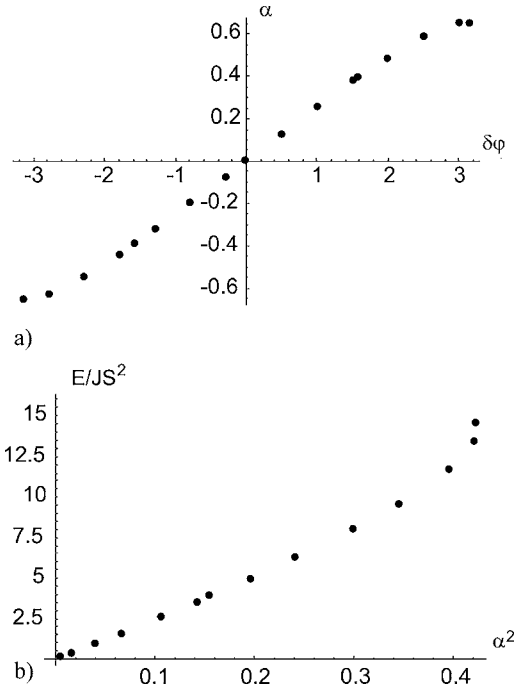


FIG. 8. Dependencies $\alpha(\delta\varphi)$ (a) and $E(\alpha^2)$ (b) for a large-distance pair ($d=10$). The agreement between the analytical model and the numerical simulation is good enough.

energy E (last two columns in the Table II) which are close to the out-of-plane values. In addition, these simulations confirm the analytical results for the energy: $E \sim \alpha^2$ and E does not depend on c . From these features we could conclude that a pinned spin in the center is a reason of appearance of logarithmic solutions both in XY and Heisenberg models.

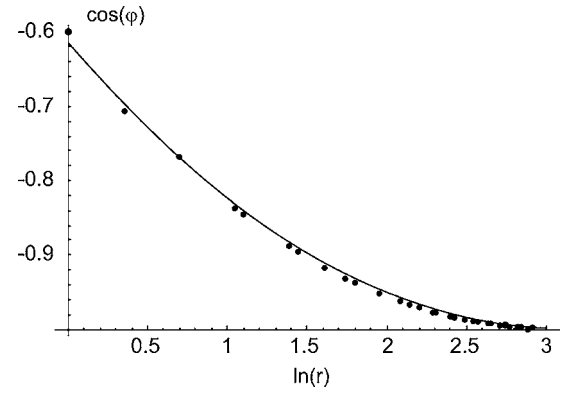


FIG. 9. Comparison of $\cos \varphi$ obtained from numerical simulation (black points) to the analytical expression $\cos \varphi = \cos\{\arctan[1.140 \tan(-0.307 \ln r + 2.544)] - \pi/2\}$ given by the continuum theory (solid line). Core spin angles are $\varphi(r_0)=1.5$ and $\theta(r_0)=0.5$.

C. Spiral vortex

In the present section we continue with simulations of a spiral vortex, and begin with the XY case. It is meaningful to investigate whether the approach described earlier keeps its validity for simulations of an ideal vortex. To perform numerical simulations we consider a square lattice of even size $2N \times 2N$ shown in Fig. 10(a) and place the vortex core in the center of the dual lattice. Then, we start with an initial configuration with $q \neq 0$ and impose free boundary condition. After 5000 iterations we reach a relaxed configuration shown in Fig. 10(b). On a lattice, the in-plane vortex angles φ_{ij} lose the perfect circular symmetry of this formula, and obtain modifications largest near the vortex core with the coordinates (\vec{i}_0, \vec{j}_0) . To check a validity of the solutions

TABLE II. Data of numerical simulations for nodal states.

$\delta\varphi = \varphi_c - \varphi_b$	$\delta\theta = \theta_c - \pi/2$	Δ_{bc}	E/JS^2	c	φ_0	R	α	α (plane)	E (plane)
1.5	0.5	1.509	1.513	1.140	$-\frac{\pi}{2}$	21.54	-0.317	-0.318	1.513
1.5	-0.5	1.509	1.513	1.140	$-\frac{\pi}{2}$	21.54	-0.317	-0.318	1.513
0.5	1.0	1.077	0.744	3.399	$\frac{\pi}{2}$	29.62	-0.227	-0.228	0.714
2.5	1.5	1.627	1.758	23.58	$\frac{\pi}{2}$	21.69	-0.340	-0.340	1.757
0	1.509	1.509	1.513	∞	—	21.54	-0.317	-0.318	1.513

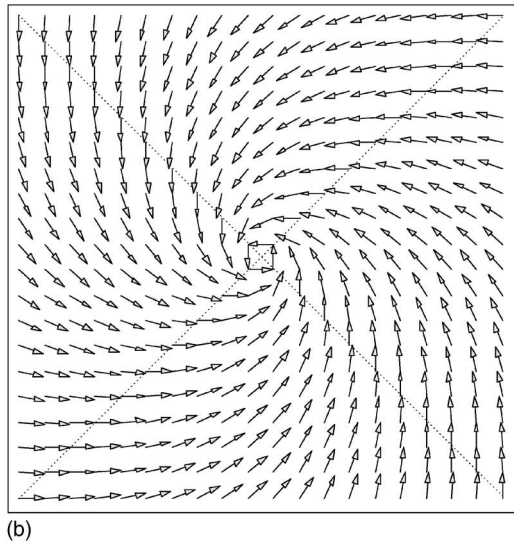
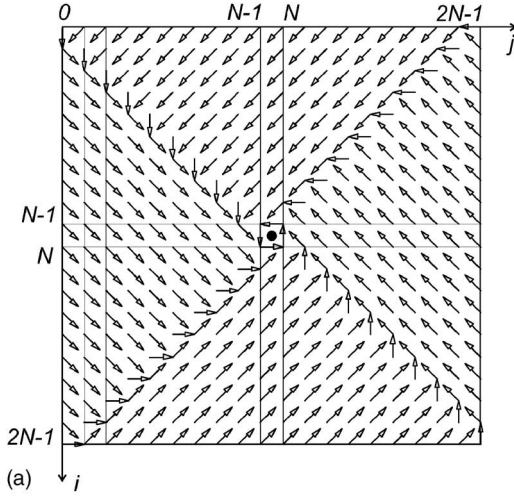


FIG. 10. Starting configuration for a simulation of vortex structures on a lattice of size $(2N, 2N)$ (a). The center with coordinates $(N-1/2, N-1/2)$ is denoted by black circle. Relaxed configuration obtained after 5000 iterations (b). The estimation of energy E/JS^2 for system of size 100×100 by using numerical codes φ_{ij} [Eq. (44)] is 16.58 vs 17.72 given by the continuum theory.

$$\cos \varphi_{ij} = \frac{i - \tilde{i}_0}{\sqrt{(i - \tilde{i}_0)^2 + (j - \tilde{j}_0)^2}}, \quad \sin \varphi_{ij} = \frac{j - \tilde{j}_0}{\sqrt{(i - \tilde{i}_0)^2 + (j - \tilde{j}_0)^2}} \quad (48)$$

we control a fulfillment of a discrete lattice nonlinear Laplace equation

$$\sum_n \sin(\varphi_p - \varphi_n) = 0,$$

where n runs over the nearest neighbors of the p th site, with an accuracy of order 10^{-2} in the center and 10^{-5} at the outskirts.

As a next step, we perform numerical simulations for a spiral vortex determined by the most common expression for the harmonic function

$$a(x, y) = q \arctan \frac{y - \tilde{y}_0}{x - \tilde{x}_0} + \alpha \ln \frac{\sqrt{(x - x_0)^2 + (y - y_0)^2}}{R}.$$

Here we briefly review how this procedure has been organized. Assuming the vortex is placed at some position centered in a plaquette and a logarithmic source position coincides with one of the lattice sites the parameters \tilde{x}_0, \tilde{y}_0 (x_0, y_0) are chosen in the dual (direct) lattice. First, we consider an initial vortex configuration, where one of the spins nearest to the vortex is considered as a site of logarithmic source. The in-plane angle of this core site is not changed by the iteration procedure, and a fixed boundary condition holds. Farther from the core the relaxed spin angles must well be described by the continuum formula $\varphi(x, y) = q\phi + \alpha \ln(r/R)$, then we expect the spin configuration

$$\varphi_{ij} = q \arctan \frac{j - N + 1/2}{i - N + 1/2} + \alpha \ln \frac{\sqrt{(i - x_0)^2 + (j - y_0)^2}}{R}$$

would be seen to develop.

We investigate system of size 101×101 . The starting deviation $\varphi(\vec{r}_0)$ of the core spin in the uniform background results in the relaxed configuration with α and the energy E [Fig. 11(a)]. Most importantly, we observe a logarithmic dependence of the in-plane angles φ_{ij} for scans (used further in the fitting to determine α values) along paths in definite directions [Fig. 11(b)] while scans along another directions shows the opposite feature [Fig. 11(c)]. This procedure has been repeated at several different positions of the fixed spin (x_0, y_0) and the results are shown in Table III, where in the last column we show the α values derived from the calculated energy E .

This is done by using the expression $E = E_{\log} + E_{\text{vort}}$, where

$$E_{\log} = \pi JS^2 \alpha^2 \ln \frac{L}{a}, \quad E_{\text{vort}} = \pi JS^2 q^2 \ln \frac{L}{a},$$

for the spiral vortex energy in the continuum approximation which is suggested to be valid. The value for $E_{\text{vort}}/JS^2 = 16.58$ is taken from the simulations of the ideal vortex. With this general expression, where $E_{\text{vort}}/E_{\log} = q^2/\alpha^2$, it is easy to find α which will be given by $\alpha(\text{energy}) = \sqrt{(E - E_{\text{vort}})/E_{\text{vort}}}$. The following features are evident from Table III.

(1) The farther the fixed spin from a vortex center the closer an additional energy $E - E_{\text{vort}}$ (second column) to value found for a fixed spin in the uniform background. The region of continuum theoretical description decreases that is in agreement with the simulations for two opposite logarithmic sources already reported in Sec. III B 2.

(2) The strength α depends both on $\varphi(\vec{r}_0)$ value and a position of the fixed spin. The closer latter to a vortex center the less α at fixed $\varphi(\vec{r}_0)$ value. Far from the vortex source the parameter α becomes exactly equal to value found for one logarithmic source with the same lattice size and starting deviation $\varphi(\vec{r}_0)$.

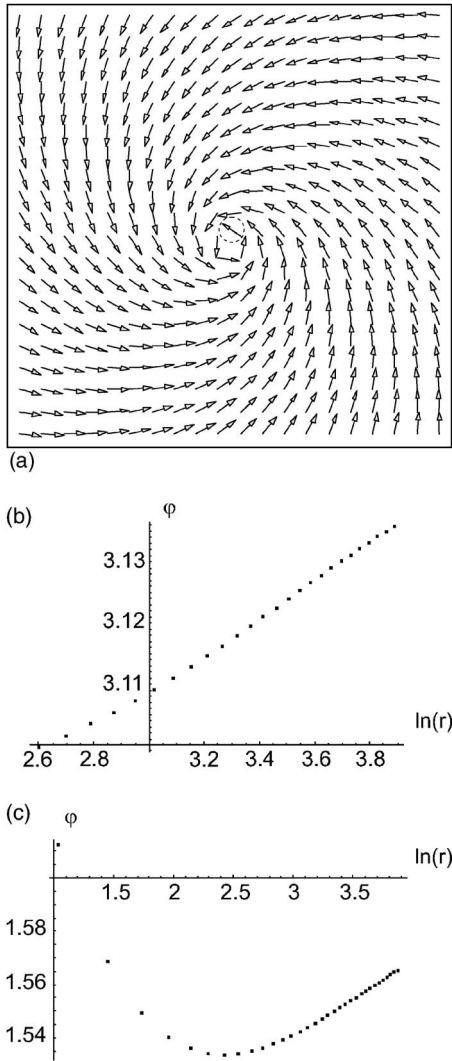


FIG. 11. Relaxed spiral-vortex configuration with the energy $E/JS^2=16.6994$. Pinned (N,N) -spin is denoted by the dotted circle (a). Dependencies of the in-plane angles φ_{ij} along the $(-1,-1)$ (b) and $(1,-1)$ (c) directions with logarithmic and nonlogarithmic behavior, respectively.

(3) The prediction of continuum theory $E \sim (\alpha^2 + q^2)$ is full reproduced by simulations for any logarithmic source and vortex positions. The lowest energy value is obtained for the smallest distance between the vortex center and the fixed spin.

D. Space spiral vortex

We begin with the case $\alpha=0$. To obtain this kind of spin structures we solved Eqs. (27), (28), and (31) by first setting

TABLE III. Data of numerical simulations for spiral vortex.

(x_0, y_0)	$(E - E_{\text{vortex}})/JS^2$	α	$ \alpha $ (energy)
(N, N)	0.114	-0.084	0.0828
$(N+5, N)$	0.554	-0.179	0.183
$(N+10, N)$	0.562	-0.182	0.184
$(N+15, N)$	0.568	-0.189	0.185

TABLE IV. Data of numerical simulations for space vortex.

c	E
1.0	2.107
1.5	2.107
3.5	2.107

the angles to their continuum values (20) and then iteratively setting each spin components to point along the direction of the effective field due to its neighbors. However, an attempt to obtain the space vortex by this way on the full square or disk fails. For these systems the iteration procedure either converges to a Skyrmion structure (free boundary conditions) or does not converge at all when the boundary spins held fixed. The reason is the iteration procedure relaxes to a minimal energy state. Since the feature of a starting configuration employed in numerical calculations is a nonzero angular momentum, this configuration may evolve either into the Skyrmion-like or into the space vortexlike structures. However, the former has a gain in energy in comparison with the last one. To avoid this difficulty we consider a simple way in which the Skyrmion structure loses the advantage. Noting that an essential contribution to the vortex energy comes from the spins within a small-radius core we takes the computational region in the form of ring with the inner radius R_1 and the external radius R_2 . This results in small differences of the discrete solution from the continuum result (20).

We found the energy for the different parameters c as shown in Table IV for the ring of size $R_1=50.5$ and $R_2=105.5$ with free boundary conditions. In full agreement with the continuum theory these energies have no dependence on c values. In Table V we listed the space vortex energy as a function of the inner radius R_1 at fixed $R_2=100.5$. We see that agreement between the numerical and the continuum theory result $E = \pi JS^2 \ln(R_2/R_1)$ is nice for the whole range of radius $10.5 \leq R_1 \leq 50.5$. We may conclude that in the system without a finite-radius core the space vortex will have the lowest energy among solutions with a non-zero angular momentum. This assertion is supported by direct analytical consideration.³⁸

Now we turn to the space spiral vortex with $\alpha \neq 0$. To obtain this configuration spins belonging to both boundaries of the ring are held fixed. The constants $\phi_0(R_1)$ and $\phi_0(R_2)$ should be taken different (“twisted” boundary conditions).

TABLE V. Space vortex energy as a function of the inner radius R_1 .

R_1	E (lattice)	$E = \pi JS^2 \ln \frac{R_2}{R_1}$
10.5	7.05	7.10
20.5	4.93	5.00
30.5	3.68	3.75
40.5	2.80	2.86
50.5	2.11	2.16

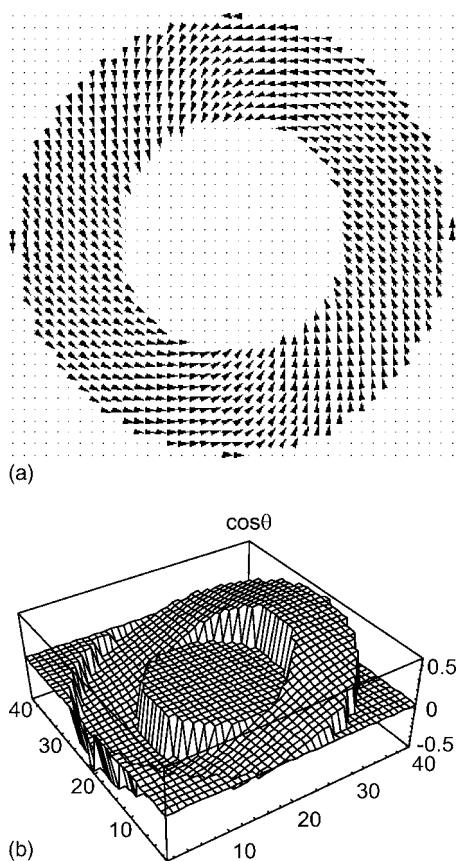


FIG. 12. Space spiral vortex ($c=2$): arrangement in the plane xy (a) and the $\cos \theta$ profile (b).

Figure 12 presents the results of the modeling for $R_1=50.5$, $R_2=105.5$ and $\phi_0(R_2)=\phi_0(R_1)+\pi/4$ resulting in a spiral vortex structure with the energy $E=2.37JS^2$.

Recently, the statics and dynamics of flat circular magnetic nanostructures with an in-plane magnetic vortex configuration has been investigated within the framework of the Landau-Lifshitz-Gilbert equation putting particular emphasis on the polarization of the vortex center and on the in-plane vorticity.⁴⁰ Studying fast switching process induced by out-of-plane field pulses, the authors was no longer dealing with

a vortex state, but rather with a spiral (see Fig. 12 in Ref. 40). They found also that in nanorings with an inner radius R_1 and an outer radius R_2 the stability of the vortex state is enhanced, and concerning the switching of the vorticity, the nanorings have similar properties as circular ones, i.e., with $R_1=0$.

In summary, we have studied a class of spiral vortex-type solutions in a 2D Heisenberg ferromagnet and performed numerical simulations for various spiral vortex configurations using fixed twisted boundary conditions and pinned core spins (“superinstanton” boundary conditions). These simulations show a reasonable agreement with the continuum-approximation results. Based on the investigation we may identify among the nonlinear excitations the modes with circular nodes (“nodal” solutions³⁷) and modes with azimuthal nodes of magnetization M_z (space spiral vortex) that resembles the classification of magnetostatic modes excited by a magnetic-field pulses and observed recently in micron-sized ferromagnetic disks. Incidentally, only axially symmetric magnetostatic modes appeared if the tipping pulse is uniform over the disk and all geometries are perfectly axially symmetric. Symmetry breaking modes, instead, required, e.g., a nonuniform tipping pulse having a sizable gradient in the plane of the vortex or a deviation of the sample from a perfect cylindrical shape.²² However, the frequency of non-axially symmetric magnetostatic modes has a negative dispersion, i.e., it decreases with a growth of a number of azimuthal nodal lines. Unlike this, for the nonlinear excitations, which are of exchange origin, a number of these lines coincides with a number of spiral arms (or with the vortex topological charge q) and increases the energy. These stationary nonlinear modes must be taken into account for yielding a better understanding, e.g., the fast magnetic switching properties in magnetic memory materials.

ACKNOWLEDGMENTS

We would like to thank B. A. Ivanov and M. V. Sadovskii for the useful discussions. This work was partly supported by Grant No. NREC-005 of US CRDF (Civilian Research and Development Foundation) and by RFBR Grant No. 03-01-00100.

¹*Nonlinearity in Condensed Matter*, edited by A. R. Bishop, R. Ecke, and S. Gubernatis (Springer, Berlin, 1993).

²*Nonlinear Coherent Structures in Physics and Biology*, edited by K. H. Spatchek and F. G. Mertens (Plenum, New York, 1994).

³*Fluctuation Phenomena: Disorder and Nonlinearity*, edited by A. R. Bishop, S. Jimenez, and L. Vazquez (World Scientific, Singapore, 1995).

⁴A. A. Belavin and A. M. Polyakov, *JETP Lett.* **22**, 245 (1975).

⁵S. E. Barrett, G. Dabbagh, L. N. Pfeiffer, K. W. West, and R. Tycko, *Phys. Rev. Lett.* **74**, 5112 (1995).

⁶S. Takeno and S. Homma, *Prog. Theor. Phys.* **65**, 172 (1981).

⁷M. E. Gouvea, G. M. Wysin, A. R. Bishop, and F. G. Mertens, *Phys. Rev. B* **39**, 11 840 (1989).

⁸B. A. Ivanov and A. K. Kolezhuk, *Fiz. Nizk. Temp.* **21**, 355 (1995).

⁹A. M. Kosevich, B. A. Ivanov, and A. S. Kovalev, *Phys. Rep.* **194**, 119 (1990).

¹⁰T. Shinjo, T. Okuno, R. Hassdorf, K. Shigeto, and T. Ono, *Science* **289**, 930 (2000).

¹¹R. P. Cowburn, A. O. Adeyeye, and M. E. Welland, *Phys. Rev. Lett.* **81**, 5414 (1998).

¹²R. P. Cowburn, D. K. Koltsov, A. O. Adeyeye, M. E. Welland, and D. M. Tricker, *Phys. Rev. Lett.* **83**, 1042 (1999).

¹³R. Pulwey, M. Rahm, J. Biberger, and D. Weiss, *IEEE Trans. Magn.* **37**, 2076 (2001).

¹⁴G. Gubbiotti, G. Carlotti, F. Nizzoli, R. Zivieri, T. Okuno, and T.

- Shinjo, IEEE Trans. Magn. **38**, 2532 (2002).
- ¹⁵A. Fernandez and C. J. Cerjan, J. Appl. Phys. **87**, 1395 (2000).
- ¹⁶J. Raabe, R. Pulwey, R. Sattler, T. Schweiboeck, J. Zweck, and D. Weiss, J. Appl. Phys. **88**, 4437 (2000).
- ¹⁷A. Lebib, S. P. Li, M. Natali, and Y. Chen, J. Appl. Phys. **89**, 3892 (2001).
- ¹⁸S. O. Demokritov, B. Hillebrands, and A. N. Slavin, Phys. Rep. **348**, 441 (2001).
- ¹⁹S. B. Choe, Y. Acremann, A. Scholl, A. Bauer, A. Doran, J. Stöhr, and H. A. Padmore, Science **304**, 420 (2004).
- ²⁰J. P. Park, P. Eames, D. M. Engebretson, J. Berezovsky, and P. A. Crowell, Phys. Rev. B **67**, 020403(R) (2003).
- ²¹M. Buess, R. Höllinger, T. Haug, K. Perzlmaier, U. Krey, D. Pescia, M. R. Scheinfein, D. Weiss, and C. H. Back, Phys. Rev. Lett. **93**, 077207 (2004).
- ²²M. Buess, T. Haug, M. R. Scheinfein, and C. H. Back, Phys. Rev. Lett. **94**, 127205 (2005).
- ²³M. Buess, T. P. J. Knowles, R. Höllinger, T. Haug, U. Krey, D. Weiss, D. Pescia, M. R. Scheinfein, and C. H. Back, Phys. Rev. B **71**, 104415 (2005).
- ²⁴M. S. Gross and P. C. Hohenberg, Rev. Mod. Phys. **65**, 851 (1993).
- ²⁵F. J. Nédélec, T. Surrey, A. C. Maggs, and S. Leibler, Nature (London) **389**, 305 (1997).
- ²⁶L. A. S. Mól, A. R. Pereira, and A. S. T. Pires, Phys. Rev. B **66**, 052415 (2002).
- ²⁷S. A. Leonel, P. Z. Coura, A. R. Pereira, L. A. S. Mo'l, and B. V. Costa, Phys. Rev. B **67**, 104426 (2003).
- ²⁸G. M. Wysin, Phys. Rev. B **68**, 184411 (2003); **70**, 094423 (2004).
- ²⁹A. Patrascioiu and E. Seiler, Phys. Rev. Lett. **74**, 1920 (1995); Phys. Rev. D **57**, 1394 (1998).
- ³⁰F. Niedermayer, M. Niedermaier, and P. Weisz, Phys. Rev. D **56**, 2555 (1997).
- ³¹M. Aguado and E. Seiler, Phys. Rev. D **70**, 107706 (2004).
- ³²A. R. Pereira, S. A. Leonel, P. Z. Coura, and B. V. Costa, Phys. Rev. B **71**, 014403 (2005).
- ³³R. Balakrishnan and A. R. Bishop, Phys. Rev. B **40**, 9194 (1989).
- ³⁴A. B. Borisov, JETP Lett. **73**, 242 (2001).
- ³⁵L. M. Pismen, *Vortices in Nonlinear Fields* (Clarendon Press, Oxford, 1999).
- ³⁶A. M. Tselik, *Quantum Field Theory in Condensed Matter Physics* (Cambridge University Press, Cambridge, 1998).
- ³⁷I. G. Bostrem and A. S. Ovchinnikov, JETP Lett. **76**, 846 (2002).
- ³⁸A. B. Borisov, I. G. Bostrem, and A. S. Ovchinnikov, JETP Lett. **80**, 846 (2004).
- ³⁹R. F. Egorov, I. G. Bostrem, and A. S. Ovchinnikov, Phys. Lett. A **292**, 325 (2002).
- ⁴⁰R. Höllinger, A. Killinger, and U. Krey, J. Magn. Magn. Mater. **261**, 178 (2003).